# Radiation resistance matrix for baffled simply curved plates for sound power applications

Ian C. Bacon[a),*], Trent P. Bates[b)], Caleb B. Goates[a)], Micah R. Shepherd[a)], Jonathan D. Blotter[b)] and Scott D. Sommerfeldt[a)]

(Received: 5 October 2023; Revised: 1 February 2024; Accepted: 12 February 2024)

**Sound power, a standard metric used to quantify product noise, is determined through the vibration-based sound power (VBSP) method. This method involves measuring surface velocities and utilizing an acoustic radiation resistance matrix, R, dependent on the structure's geometry. While R matrix expressions have been established for baffled flat plates, fully closed cylinders, and fully closed spheres, this work presents the first analytical expression tailored for baffled simply curved plates with uniform curvature. This development, based on eigenfunction expansion and the uniform theory of diffraction, extends the VBSP method's capabilities for accurate sound power assessment from these structures. Experimental validation involved testing three plates of varying curvature in a reverberation chamber, comparing the VBSP method with the ISO 3741 pressure-based standard. One of the curved plates underwent additional testing in an anechoic chamber following the ISO 3745 standard, confirming the VBSP method's accurate sound power measurements down to the 160 Hz one-third octave band. The same plate was tested in uncontrolled acoustic environments — a busy hallway and an outdoor location. The VBSP results showed strong agreement with ISO 3741, affirming the method's robustness for measuring sound power from baffled simply curved plates in acoustically challenging real-world conditions. This underscores the practicality of the VBSP method, enabling accurate sound power measurements of baffled curved plates in the presence of substantial background noise and environmental variability.** 

Primary subject classification: 72.4; Secondary subject classification: 21.2.1

## 1 INTRODUCTION

Sound power is a widely used metric for comparing radiated noise levels across various products, from home appliances to construction vehicles. Many existing standards for sound power measurement require specific acoustic environments, such as anechoic and reverberation chambers, which are cost prohibitive. Consequently, designers often do not have sound power data to effectively prioritize noise reduction in product development. Vibration-based sound power (VBSP) measurement methods offer a potential solution by reducing the constraints of acoustic environments and the associated costs, making sound power measurements more feasible for designers to utilize sound power data to develop quieter products.

[a)] Department of Physics and Astronomy, Brigham Young University, Provo, UT 84602, USA; Emails: calebgoates@gmail.com, micah_shepherd@byu.edu, scott_sommerfeldt@byu.edu.
[b)] Department of Mechanical Engineering, Brigham Young University, Provo, UT 84602, USA; Emails: tbateslefty24@gmail.com, jblotter@byu.edu
* Corresponding author. Email: icbacon@byu.edu.

The foundational theory for computing sound power using vibration-based methods is often referred to as the method of elementary radiators, which originated in the early 1990s[1–4]. In this method, the structure is discretized into an array of small individual radiators, and the velocity of each radiator is measured. Using a radiation resistance matrix, **R**, the sound power is computed as

$$\Pi(\omega) = \mathbf{v}_e^H(\omega)\mathbf{R}(\omega)\mathbf{v}_e(\omega) \tag{1}$$

where $\mathbf{v}_e$ is a vector of the velocity of each individual radiator, $(\cdot)^H$ is the Hermitian transpose, and $\omega$ is the frequency[2,5].

Arenas described the **R** matrix as a transfer function linking the surface normal velocities of a structure to the acoustic pressures on the surface of each radiator[6]. The individual terms in the **R** matrix, $R_{pq}$, represent the radiation resistance on radiator $p$ due to radiator $q$. Thus, the **R** matrix is a square symmetric matrix where both the rows and columns equal the number of radiators, and the number of elements is equal to the total number of radiators squared.

The **R** matrix is primarily a function of the acoustic pressure propagation distances between the individual radiators, leading to different expressions for these distances between flat and curved geometries.

Historically, acoustic radiation modes were derived from the **R** matrix corresponding to a specific geometry and then utilized to compute sound power[1–4] or as a tool to improve structural design and active noise control techniques[7]. Radiation modes explain how the vibrational energy of a structure transforms into acoustic energy by analyzing the distribution of velocity across its surface[2,8,9]. Goates et al.[10] previously referred to this method as the vibration-based radiation mode (VBRM) method[11]. Cunefare and Currey[4] showed the convergence of a sufficient number of these modes to obtain good resolution for the sound power within a given range.

It was found within this work that when higher frequencies are of interest, using radiation modes to compute sound power does not yield significant computational savings compared to simply using the entire **R** matrix and computing the matrix multiplication in Eqn. 1. This is primarily due to the extensive computations required to determine the radiation modes, often comparable to directly calculating the sound power using the full **R** matrix. This method of using the full **R** matrix to compute sound power is referred to as the VBSP method[12]. Convergence for sound power results using the VBSP method can be obtained by ensuring sufficient spatial resolution when discretizing the surface of interest. Although this method will only utilize the **R** matrix, the acoustic radiation modes of simply curved plates can be obtained for other applications by performing singular value decomposition on the **R** matrix, developed later in this work.

Previous research has established analytical expressions for the radiation resistance matrix for flat plates[2,5,11–13], fully closed cylindrical shells[10,14–18], and fully closed spherical shells[1,18–19]. In these fully closed geometries, the acoustic pressure from one radiator can propagate to another by traversing the surface of the structure in multiple directions as well as going around the structure several times. Many common geometries, including car door panels, windshields, aircraft fuselage panels, and engine covers, do not fit these existing models. Therefore, there is a need for a validated expression for the **R** matrix that can accurately model simply curved-plate geometries.

Bates et al.[20] have shown that some baffled arbitrarily-curved panels can be approximated using one of the known forms of the **R** matrix mentioned earlier. However, limitations exist in this approach, particularly regarding the radius of curvature and the coupling between radiators that exists within a certain range of frequencies. While Bates et al.[20] provided an analytical expression for the **R** matrix of baffled simply curved plates, no theoretical development or validation of this expression is available in the existing literature. This knowledge gap presents a challenge for groups seeking to understand the natural acoustic radiation from these simply curved plates, whether for sound power computation or active noise control. It is crucial to address these limitations and verify the accuracy of the expression numerically or experimentally to validate this expression.

The purpose of this work is to fill this critical research gap by presenting and validating, for the first time, the theoretical development of the **R** matrix for baffled simply curved plates. This development is based on the eigenfunction expansion and the uniform theory of diffraction to determine the distances between every elementary radiator and how the acoustic radiation is produced and transferred from these geometries. This work only considers simply plates with a single constant radius of curvature, deviating from fully closed geometries like cylinders and spheres.

This work will then show experimental results validating the analytical expression for this **R** matrix and enable the extension of the VBSP method to accurately account for simply curved plates. Experimental validation was conducted through comparing VBSP results with sound power measurements obtained following the ISO 3741 and ISO 3745 standards[21,22], which are well-established sound pressure measurement-based standards. By providing a validated expression and expanding the applicability of the VBSP method, an accurate assessment of the sound radiation from simply curved plates can be facilitated, benefiting various industries and applications.

## 2 CURVED PLATE RADIATION RESISTANCE MATRIX THEORY

The **R** matrix for a simply curved plate is obtained by initially deriving the **R** matrix for a fully closed cylinder. This section begins with a concise overview of the derivation process for the **R** matrix of the fully closed cylinder, followed by the derivation for open simply curved plates. Subsequently, the expression is further simplified for more efficient computation by using the uniform theory of diffraction.

### 2.1 Simply Curved Plate Radiation Resistance Matrix

The **R** matrix is derived from the acoustic pressure that a small vibrating element of a structure generates across the structure. The general form of the **R** matrix for the $pq$th element can be expressed as a function of the pressure as given by[4,23]

$$R_{pq} = \frac{S_e}{2u_0}\,\mathrm{Re}\left\{p_q\left(a\theta_p, z_p\right)\right\} \tag{2}$$

where $S_e$ is the area of the vibrating element or radiator given by $S_e = a\Delta\theta\Delta z$, $u_0$ is the velocity amplitude of the $q$th element, $p_q(a\theta_p, z_p)$ is the pressure generated at the $p$th location by vibration at the $q$th location, $a$ is the radial distance (radius of curvature) for the surface of the curved structure, and $\theta_p$ and $z_p$ are the physical coordinates of the $p$th location.

Consider a rigid infinite cylinder of radius $a$ as shown in Fig. 1. Assume that a small rectangular patch or radiator on the cylinder with circumferential extent $\Delta\theta$ and height $\Delta z$ is vibrating with a surface normal velocity $u_0$, such that there is effectively a simple source of strength $u_0 a\Delta\theta\Delta z$ at $(r, \theta, z) = (a\theta_p, z_p)$. This vibration creates a pressure field over the structure that can be written as[23]

$$p_q(r, \theta, z) = \sum_{m=-\infty}^{\infty} \int_{-\infty}^{\infty} A_m(k_z) e^{jk_z z} e^{jm\theta} H_m^{(2)}(k_r r) dk_z, \tag{3}$$

where $A_m(k_z)$ is unknown coefficients, $H_m^{(2)}(k_r r)$ is the $m$th-order Hankel function of the second kind (defined in appendix A by Eqn. A.4), $j = \sqrt{-1}$, $m$ is an integer, $k_z$ is the axial wavenumber, and $k_r = \sqrt{k^2 - k_z^2}$, where $k$ is the acoustic wavenumber. The pressure is defined for each radiator, and the pressure field is represented by a vector the length of the number of radiators. Therefore, a single subscript is used to define the pressure.

The surface velocity may be expanded in terms of the $\theta$ and $z$ eigenfunctions as

$$u_q(\theta, z) = \left(\frac{u_0\Delta\theta\Delta z}{4\pi^2}\right) \sum_{m=-\infty}^{\infty} \int_{-\infty}^{\infty} e^{jk_z(z-z_q)} e^{jm(\theta-\theta_q)} dk_z \tag{4}$$

from which the pressure expression coefficients may be solved for by applying the surface condition at $r = a$,

$$\frac{\partial p_q}{\partial r}|_{r=a} = -j\omega\rho_0 u_q(\theta, z) \tag{5}$$

Applying these steps and simplifying give the pressure as

$$p_q(r, \theta, z) = -j\left(\frac{\omega\rho_0 u_0\Delta\theta\Delta z}{4\pi^2}\right) \sum_{m=-\infty}^{\infty} e^{jm(\theta-\theta_q)} \int_{-\infty}^{\infty} \frac{H_m^{(2)}(k_r a)}{H_m^{(2)'}(k_r a)} e^{jk_z(z-z_q)} \frac{dk_z}{k_r} \tag{6}$$

where the prime denotes a derivative with respect to the argument. Using Euler's formula, this can be written in terms of trigonometric functions instead of exponentials as

$$p_q(r, \theta, z) = -j\left(\frac{\omega\rho_0 u_0\Delta\theta\Delta z}{\pi^2}\right) \sum_{m=0}^{\infty} \cos[m(\theta - \theta_j)] \int_{0}^{\infty} \frac{H_m^{(2)}(k_r a)}{H_m^{(2)'}(k_r a)} \cos[k_z(z - z_j)] \frac{dk_z}{k_r} \tag{7}$$

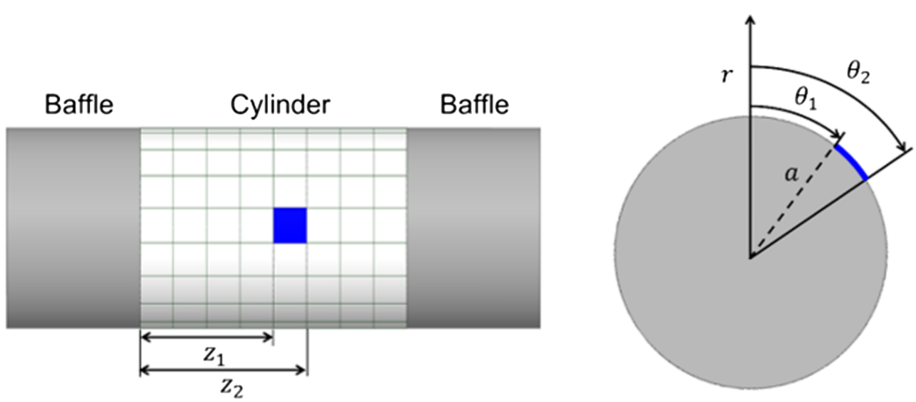


*Fig. 1—Schematic of the infinitely baffled cylinder geometry. The non-rigid portion of the cylinder is discretized, and the radiator described in Eqn. 3 is highlighted in blue (left). An end view of the cylinder of radius a shows the dimensions of an arbitrary element, represented by the length $z_2 - z_1$ and width $a(\theta_2 - \theta_1)$ (right).*

The $pq$th element of the **R** matrix can then be expressed by substituting Eqn. 7 into Eqn. 2 as given by

$$\begin{aligned} R_{\text{cyl},pq} &= \frac{S_e}{2u_0}\,\text{Re}\{p_q(a\theta_p, z_p)\} \\ &= \text{Re}\left\{-j\left(\frac{\omega\rho_0 S_e^2}{2\pi^2 a}\right)\sum_{m=0}^{\infty}\cos\left[m(\theta-\theta_j)\right]\int_0^{\infty}\frac{H_m^{(2)}(k_r a)}{H_m^{(2)'}(k_r a)}\cos\left[k_z(z-z_j)\right]\frac{dk_z}{k_r}\right\} \\ &= \left(\frac{\omega\rho_0 S_e^2}{2\pi^2 a}\right)\sum_{m=0}^{\infty}\cos\left[m(\theta-\theta_j)\right]\int_0^{\infty}\text{Re}\left\{-\frac{j}{k_r}\frac{H_m^{(2)}(k_r a)}{H_m^{(2)'}(k_r a)}\right\}\cos\left[k_z(z-z_j)\right]dk_z, \end{aligned} \tag{8}$$

which can be further simplified by recognizing that the Hankel functions ratio becomes imaginary for imaginary $k_r$. This simplification reduces the integration in $k_z$ from 0 to $k$, giving the final form

$$R_{\text{cyl},pq} = \frac{\omega\rho_0 S_e^2}{2\pi^2 a}\sum_{m=0}^{\infty}\cos\left[m(\theta_p-\theta_q)\right]\int_0^{k}\frac{1}{k_r}\,\text{Im}\left\{\frac{H_m^{(2)}(k_r a)}{H_m^{(2)'}(k_r a)}\right\}\cos\left[k_z(z_p-z_q)\right]dk_z. \tag{9}$$

In addition to this fully closed cylinder expression, eigenfunction expansion can give the **R** matrix for a partial cylinder radiating into a partial cylindrical space as shown in Fig. 2. The main difference is the application of a Neumann boundary condition at $\theta = 0$ and $\theta = \theta_L$ where $\theta_L$ is the angular extent of the space instead of the periodicity requirement on $\theta$. Making these changes results in the following expression for a partial cylinder or simply curved plate[9]

$$R_{\text{part cyl},pq} = \frac{\omega\rho_0 S_e^2}{\pi a\theta_L}\sum_{m=0}^{\infty}\cos\left(\frac{m\pi\theta_p}{\theta_L}\right)\cos\left(\frac{m\pi\theta_q}{\theta_L}\right)\int_0^{k}\frac{1}{k_r}\,\text{Im}\left\{\frac{H_m^{(2)}(k_r a)}{H_m^{(2)'}(k_r a)}\right\}\cos\left[k_z(z_p-z_q)\right]dk_z. \tag{10}$$

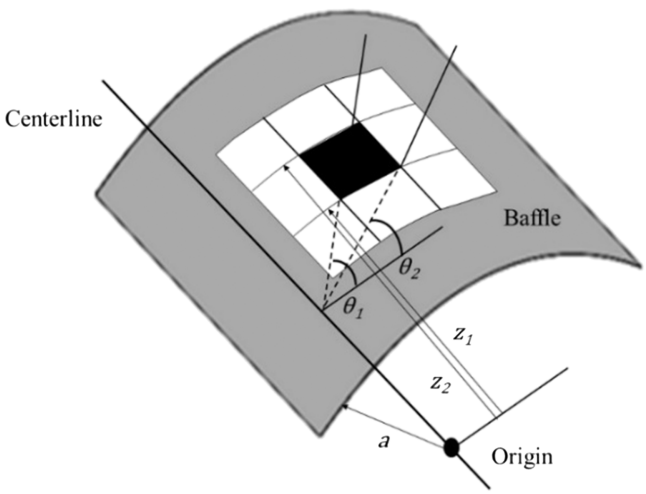


*Fig. 2—The geometric values and the area of an element in the baffled curved plate are shown. These elements represent the radiators that produce the pressure at the pth location in response to vibration at the qth location.*

The drawbacks to this expression are the infinite sum and the integrals which can be overcome as shown in the following section using the uniform theory of diffraction.

## 2.2 Uniform Theory of Diffraction

Although **R** matrix formulations could be derived directly from Eqns. 9 and 10, these equations involve computationally expensive infinite sums and integrals. For cylindrical structures with large radii of curvature, Eqn. 9 can be further simplified by applying principles from the uniform theory of diffraction. Initially developed in electromagnetics, this approach to wave propagation around curved surfaces has had limited application in acoustics[24–27]. The formulation can be obtained by employing an asymptotic expansion of Eqn. 6 for large $ka$ values. After evaluation at $r = a$ and substituting $\phi = \theta - \theta_q$, Eqn. 6 can be written as

$$p_q(a,\theta,z) = -j\left(\frac{\omega\rho_0 u_0 \Delta\theta\Delta z}{4\pi^2}\right)\int_{-\infty}^{\infty}dk_z\frac{e^{jk_z(z-z_q)}}{k_r}\sum_{m=-\infty}^{\infty}\frac{H_m^{(2)}(k_r a)}{H_m^{(2)'}(k_r a)}e^{jm\phi}. \tag{11}$$

The sum in this expression can be transformed into an integral in the complex plane by using a Watson transformation[27–29], as follows:

$$\sum_{m=-\infty}^{\infty} \frac{H_m^{(2)}(k_r a)}{H_m^{(2)'}(k_r a)} e^{jm\phi} = \frac{j}{2} \int_C \frac{e^{jv(\phi-\pi)}}{\sin v\pi} \frac{H_v^{(2)}(k_r a)}{H_v^{(2)'}(k_r a)} dv, \tag{12}$$

where $C$ is a contour that encircles the real axis. Then, by replacing $-v$ by $v$ in the part of the contour above the axis, the right-hand side of Eqn. 12 becomes

$$\sum_{m=-\infty}^{\infty} \frac{H_m^{(2)}(k_r a)}{H_m^{(2)'}(k_r a)} e^{jm\phi} =$$

$$\frac{j}{2} \int_{-\infty-j\varepsilon}^{\infty-j\varepsilon} \frac{\cos v(\phi-\pi)}{\sin v\pi} \frac{H_v^{(2)}(k_r a)}{H_v^{(2)'}(k_r a)} dv. \tag{13}$$

Then, by replacing the trigonometric terms with their equivalent exponential terms yields

$$\sum_{m=-\infty}^{\infty} \frac{H_m^{(2)}(k_r a)}{H_m^{(2)'}(k_r a)} e^{jm\phi} =$$

$$\frac{j}{2} \int_{-\infty-j\varepsilon}^{\infty-j\varepsilon} \frac{e^{-jv(2\pi-\phi)} + e^{-jv\phi}}{1 - e^{-jv2\pi}} \frac{H_v^{(2)}(k_r a)}{H_v^{(2)'}(k_r a)} dv. \tag{14}$$

Next, a geometric series can be used to obtain

$$\sum_{m=-\infty}^{\infty} \frac{H_m^{(2)}(k_r a)}{H_m^{(2)'}(k_r a)} e^{jm\phi} =$$

$$\frac{j}{2} \int_{-\infty-j\varepsilon}^{\infty-j\varepsilon} \frac{H_v^{(2)}(k_r a)}{H_v^{(2)'}(k_r a)} \sum_{\ell=0}^{\infty} \left( e^{-jv(2\pi-\phi)} + e^{-jv\phi} \right) e^{-j2\pi\ell v} dv. \tag{15}$$

Equation 15 can be interpreted as a summation of waves that have encircled the cylinder $\ell$ times, composed of separate terms for waves circling in a positive direction and waves circling in a negative direction. By assuming that $k_r a$ is large and recognizing that the greatest contribution to the integral occurs near $v = k_r a$, all but the $\ell = 0$ terms can be neglected[25]. This simplification yields the final quantity as

$$\sum_{m=-\infty}^{\infty} \frac{H_m^{(2)}(k_r a)}{H_m^{(2)'}(k_r a)} e^{jm\phi} \approx \frac{j}{2} \int_{-\infty-j\varepsilon}^{\infty-j\varepsilon} \frac{H_v^{(2)}(k_r a)}{H_v^{(2)'}(k_r a)} \left( e^{-jv(\phi-2\pi)} + e^{-jv\phi} \right) dv. \tag{16}$$

Considering that the integral over $v$ is primarily influenced by $v = k_r a$, Pathak and Wang[25] proposed the substitution $v = k_r a + \tau (k_r a/2)^{1/3}$, with $\tau$ as the new independent variable. Following this asymptotic formulation suggested by Pathak and Wang,[25] the sum in Eqn. 12 can be expressed as

$$\sum_{m=-\infty}^{\infty} \frac{H_m^{(2)}(k_r a)}{H_m^{(2)'}(k_r a)} e^{jm\phi} =$$

$$-\frac{j}{2} \int_{-\infty}^{\infty} \left( \frac{k_r a}{2} \right)^{1/3} \frac{W_2(\tau)}{W_2'(\tau)} e^{-jv\phi} d\tau, \tag{17}$$

where $W_2(\tau)$ represents one of the Airy-Fock functions[30] (defined in Appendix A by Eqn. A.5). Furthermore, it should be noted that employing $e^{-jv\phi}$ in the integral accounts for a single ray traveling in one circumferential direction along the cylindrical surface. Substituting $v$ and this result back into Eqn. 11 yields the surface pressure as[23]

$$p_q(r, \theta, z) = -\frac{\omega \rho_0 u_0 \Delta\theta \Delta z}{8\pi^2} \int_{-\infty}^{\infty} \frac{e^{j\left[k_z(z-z_q)+k_r a\phi\right]}}{k_r} dk_z \int_{-\infty}^{\infty} \left( \frac{k_r a}{2} \right)^{1/3} \frac{W_2(\tau)}{W_2'(\tau)} e^{-j\phi\left(\frac{k_r a}{2}\right)^{1/3}\tau} d\tau. \tag{18}$$

The first integral (over $k_z$) can be evaluated using a polar transformation, resulting in the expression for the pressure from this single ray being written as

$$p_q(t) = \frac{j\omega \rho_0 u_0 S_e}{2\pi} V(\xi) \frac{e^{-jk\eta}}{\eta}, \tag{19}$$

where

$$V(\xi) = \left( \frac{\xi}{4\pi} \right)^{1/2} e^{\frac{j\pi}{4}} \int_{-\infty}^{\infty} d\tau \, \frac{W_2(\tau)}{W_2'(\tau)} \, e^{-j\xi\tau}. \tag{20}$$

Equation 20 represents a simplified version of Eqn. A.6 found in Appendix A. $V(\xi)$ denotes the hard Fock coupling function with real argument $\xi = \eta[k \cos^4\psi/(2a^2)]^{1/3}$,

$\eta = \sqrt{(\Delta z)^2 + a^2(\Delta\theta)^2}$ is the distance traversed across the curved surface, and $\psi = \tan^{-1}\left(\frac{\Delta z}{a\phi}\right)$ is the angle between the direction of propagation and the cylinder axis.

Substitution of Eqn. 19 into Eqn. 2 gives the expression to compute the entries of the curved plate **R** matrix as[23]

$$R_{pq} = -\frac{\omega\rho_0 S_e^2}{4\pi d_{pq}} \operatorname{Im}\left\{V(\xi)e^{-jkd_{pq}}\right\} \tag{21}$$

where $d_{pq}$ is the distance between the $p$th and $q$th positions on the surface and is also substituted for $\eta$ in $\xi$. It is important to note that the described radiation resistance considers only a single ray. While this approach is suitable for the scenarios addressed in this work, involving baffled curved plates, a more comprehensive treatment for a complete cylinder would require combining two or more terms from Eqn. 21. This would allow for the depiction of the two opposite paths around the cylinder, from the source to the field point, as well as additional paths that propagate around the cylinder multiple times.

The hard Fock coupling function $V(\xi)$ has been characterized sufficiently, yielding useful series representations with ten or fewer terms (see Table A.1 in the appendix). Figure 3 provides a plot of $V(\xi)$. Notably, for large curvature ($a \gg 1$) and low frequency ($k \ll 1$), $\xi$ approaches zero and $V(\xi)$ approaches unity. In this case, $V(\xi)$ behaves like a $\operatorname{sinc}(kd_{pq})$ function, causing Eqn. 21 to collapse into the canonical expression for the **R** matrix of a flat plate, given by[5]

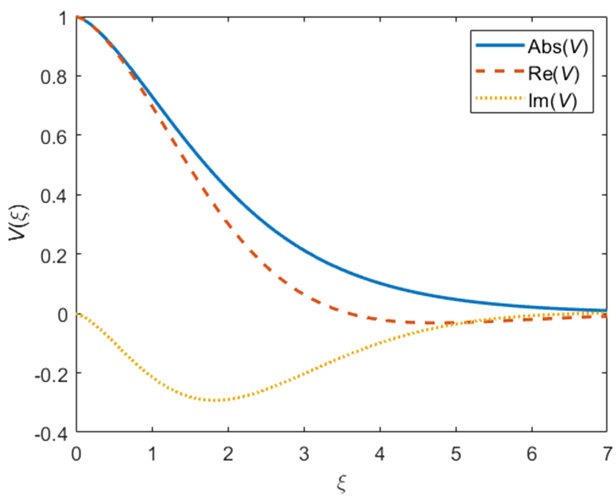


*Fig. 3—This plot shows the real part, imaginary part, and magnitude of the hard Fock V coupling function. As $\xi$ approaches zero, $V(\xi)$ behaves similarly to a $\operatorname{sinc}(kd_{pq})$ function and showcases the asymptotic behavior near zero for small curvature or large frequency.*

$$R_{\text{flat},pq} = \frac{\rho_0\omega^2 S_e^2}{4\pi c}\frac{\sin kd_{pq}}{kd_{pq}}. \tag{22}$$

Thus, the flat plate **R** matrix serves as a good approximation for these plates. On the other hand, Fig. 3 also shows that the elements of the **R** matrix for a simply curved plate, regardless of its size, tend to zero as the radius of curvature diminishes, as depicted in Eqn. 21. This occurs when $V(\xi)$ approaches zero as $\xi$ tends toward seven.

## 3 EXPERIMENTAL SETUPS FOR SOUND POWER MEASUREMENT

To confirm the accuracy of the simply curved plate **R** matrix expression, sound power measurements obtained through the VBSP method were compared with ISO 3741 and ISO 3745 standards. Experiments were conducted using three simply curved plates of varying radii in different acoustic environments: reverberant, anechoic, and uncontrolled. This section outlines the experimental setup, as well as measurement methods, and then presents the validation results.

### 3.1 Design and Setup of the Three Curved Plates

The three curved plates used during experimental testing were fabricated using the same materials and design, with the only distinguishing feature being the constant radius of curvature used. For simplicity, the curved plates in this work are identified according to their relative radius of curvature, as follows: tight radius (TR) (see Fig. 4), medium radius (MR) (see Fig. 5a), and wide radius (WR) (see Fig. 5b). The radii of curvature and other dimensions for these plates are summarized in Table 1.

Each structure has a thin aluminum sheet shaped into a curved plate with an approximately constant radius of curvature maintained in a rigid steel frame (see Fig. 4). To prevent acoustic radiation from escaping the backside of the curved plates and into the measured acoustic field, each plate is clamped on the straight edges and baffled on the curved edges using thick aluminum caps sealed to the plates with a silicone bead (see Fig. 4). Calibration marks were placed on the surface of each plate to enable a scanning laser Doppler vibrometer (SLDV) to virtually stitch scan section measurements.

### 3.2 The VBSP Method for 3D Structures

A curved plate was mounted on the wall in the specific acoustic environment, with the wall approximating an infinite baffle. Gaff tape (thick sealing tape) was applied

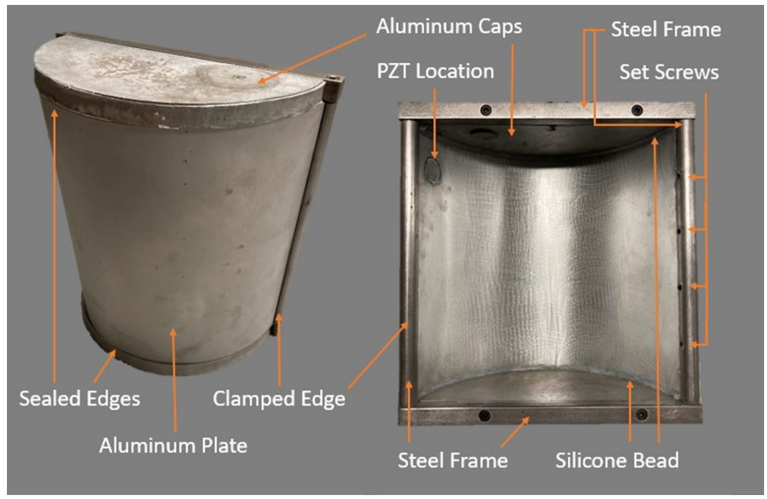


*Fig. 4—Annotated image of the TR curved plate, with the outer surface on the left and the inner surface on the right. The width corresponds to the clamped edges. Plate excitation was achieved through a PZT.*

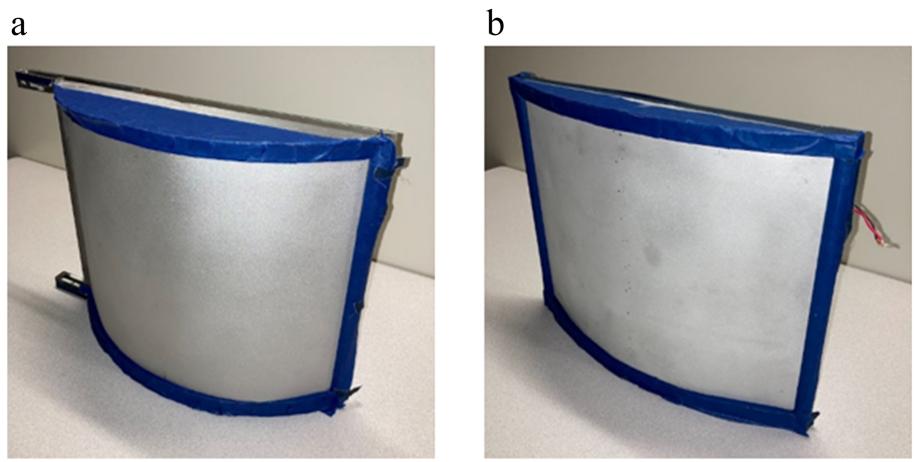


*Fig. 5—Images of (a) The MR curved plate and (b) The WR curved plate.*

around the frame-to-wall interface to ensure proper sealing and eliminate any acoustic flanking paths. The vibration and standard method measurements were made for each plate while maintaining this consistent setup.

*Table 1—Summary of curved plate dimensions used for experimental testing.*

| Object | Height (cm) | Width (cm) | Thickness (mm) | Radius of Curvature (cm) |
|---|---|---|---|---|
| TR curved plate | 30 | 29 | 1.59 | 15.5 |
| MR curved plate | 30 | 36 | 1.59 | 30 |
| WR curved plate | 30 | 40 | 1.59 | 51 |

Excitation of the plates initially involved a shaker, but there were limitations in baffling behind the plate and obstructing the view of the SLDV in front of the plate. As a solution, a piezoelectric transducer (PZT) was placed on the back side of the plate in the upper right quadrant (when facing the front). This allowed flush mounting of the plates to the chamber wall while enabling measurement of the low-frequency chamber background noise.

Structural velocity measurements were made using a Polytec PSV-500-3D SLDV equipped with three independent laser scan heads for 3D measurements. Each laser head measures the velocity along the sight of the laser beam. The software uses these three measurements to compute the three orthogonal components of velocity in the predetermined laser reference coordinate system. The

SLDV also measures the surface geometry of the plate from which an outward normal vector at each point can be determined. The surface normal velocity at each scan point is computed using the dot product,

$$V_n = \mathbf{V} \cdot \mathbf{N}, \tag{23}$$

where $V_n$ is the surface normal velocity, **V** is the 3D velocity vector, and **N** is the surface normal unit vector. Because of plate curvature, separate sections of the plate were scanned and subsequently stitched together, as seen in Fig. 6, to obtain a complete response of each simply curved plate[31].

The frequency range of interest spanned 100 Hz to 10 kHz in one-third octave (OTO) bands (89 Hz to 11,220 Hz). The scan grid density was at least six scan points per wavelength for the shortest wavelength (5.1 mm at 11,220 Hz), ensuring a spatial resolution of approximately one wavelength between each scan point in each direction and sound power measurement accuracy. A pseudo-random signal ranging from 0 to 12.8 kHz was applied to the PZT to excite each plate.

### 3.3 Reverberation Chamber and the ISO 3741 Standard

The reverberation chamber employed has dimensions of approximately 5.03 m × 5.93 m × 7.01 m with a Schroeder frequency of about 385 Hz. The sound power from the curved plates was measured and then computed using the ISO 3741 standard, which is limited to frequencies above the Schroeder frequency.

An impulse response was recorded in the reverberation chamber to factor in the additional absorption attributed to the presence of the SLDV equipment and the experimental setup. Once the absorption had been accounted for, sound pressure data were recorded using six microphones placed according to the standard. The recorded pressure data were filtered into OTO bands with a frequency bandwidth resolution of 1 Hz. Then, the vibration data and the developed curved plate **R** matrix were used to calculate sound power following the VBSP method. The obtained results are reported and compared in OTO bands with the ISO 3741 standard.

### 3.4 Anechoic Chamber and the ISO 3745 Standard

To assess the VBSP method's accuracy in measuring sound power below 385 Hz, VBSP measurements of the WR curved plate were compared with the measurements in an anechoic chamber according to ISO 3745. The chamber's anechoic properties extend down to approximately 80 Hz, allowing sound power measurements to be verified down to the 100 Hz OTO band center frequency, provided the excitation meets the specified sound pressure level to background noise criteria. To minimize the potential influence of sound wrapping around the front and affecting source measurements, a 16′ × 12′ × 3/4″; thick medium-density fiberboard (MDF) wall was constructed for mounting the WR curved plate (see Fig. 7). This wall served as a baffle, directing any radiated sound on the backside towards the anechoic terminations. It was specifically designed to mitigate the impact of the longest wavelength of interest at 89 Hz.

A directivity measurement system arc array with 36 microphones evenly spaced in 5° increments[32] was used to capture frequency response functions (FRFs) around the curved plate, covering a hemisphere along a meridional path. Each recording lasted approximately 15 seconds, with an additional 15-second settling time between rotations to minimize electrical noise from the actuator and array. The FRFs were used to calculate sound power levels from 100 Hz to 10 kHz OTO bandwidth, per the ISO 3745 standard[22].

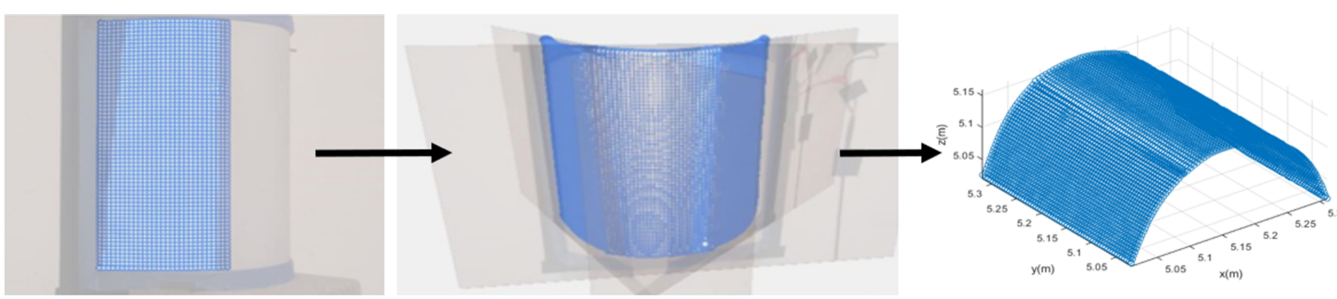


*Fig. 6—An example scan section taken over the surface of the TR curved plate to measure complex surface velocities. After each section is scanned and then stitched together to provide a complete response of the plate. During post-processing, the stitching is smoothed in case of any imperfect overlap of the sections.*

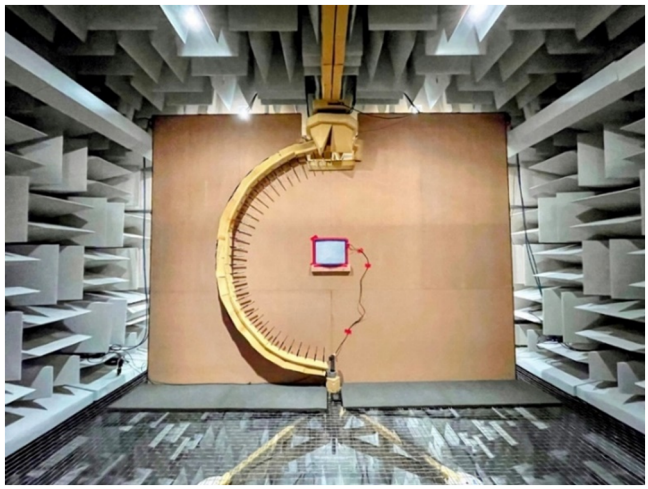

*Fig. 7—Experimental setup of the directivity measurement system (DMS) (arc array) and wall inside an anechoic chamber.*

### 3.5 The VBSP Method in Uncontrolled Acoustic Environments

To gauge the VBSP method's capability to measure radiated sound power in noisy environments outside of controlled acoustic environments, such as anechoic and reverberation chambers, experiments were conducted using the WR curved plate. The WR plate was mounted on a concrete wall at least 3-feet thick to baffle in two different locations: a hallway in BYU's Engineering Building (see Fig. 8) with moderate foot traffic, loud HVAC system, and elevator noise and an outdoor location (see Fig. 9). The outdoor setup involved challenging environmental conditions, including frequent vehicle noise, a rainstorm with thunderclaps, wind speeds up to 11 mph, and a 14° F (7.8° C) temperature change during measurement.

## 4 EXPERIMENTAL RESULTS OF SOUND POWER MEASUREMENTS

### 4.1 Reverberant (Diffuse) Environment

The Schroeder frequency was shifted down to approximately 350 Hz due to the presence of additional absorption within the reverberation chamber, placing it within the 315 Hz OTO band. Figures 10a and 10b show the sound power measurements from the TR and WR curved plates, respectively, using both the VBSP and ISO 3741 methods in a reverberation chamber. Excellent agreement was obtained between both methods between the 315 Hz to 10 kHz OTO bands.

Using a reference of $10^{-12}$ W, the overall sound power level for the TR curved plate was measured as 70.7 dB using the VBSP method and 70.2 dB using the ISO 3741 method, resulting in a difference of 0.5 dB. Similarly, for the WR curved plate, the overall sound power level was 81.0 dB using VBSP and 80.0 dB using ISO 3741, resulting in a difference of 1.0 dB.

Table 2 quantifies the OTO band sound power differences between the methods for these plates. The ISO 3741 method introduces significant error below the 315 Hz OTO band due to the noise floor, while the VBSP method demonstrates greater accuracy within this frequency range.

According to ISO 3741, if the noise floor is within 10 dB of the measured sound power, the results represent an upper bound on sound power[21]. The ISO 3741 standard depends on microphones to measure the acoustic

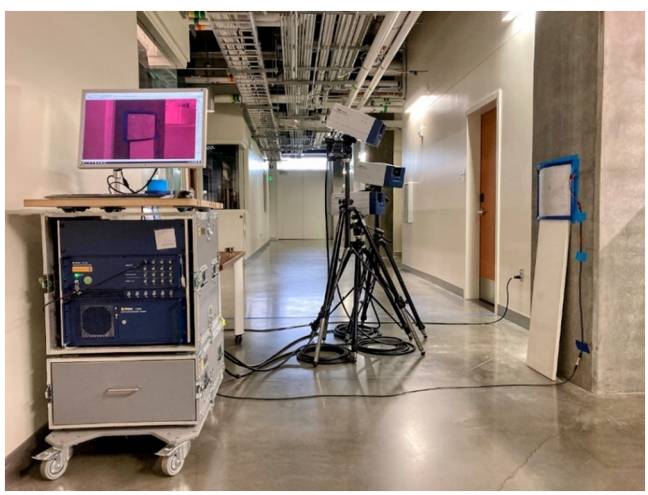

*Fig. 8—Experimental setup of the WR curved plate in a hallway inside BYU's engineering building.*


*Fig. 9—Experimental setup of the WR curved plate outside of BYU's engineering building.*

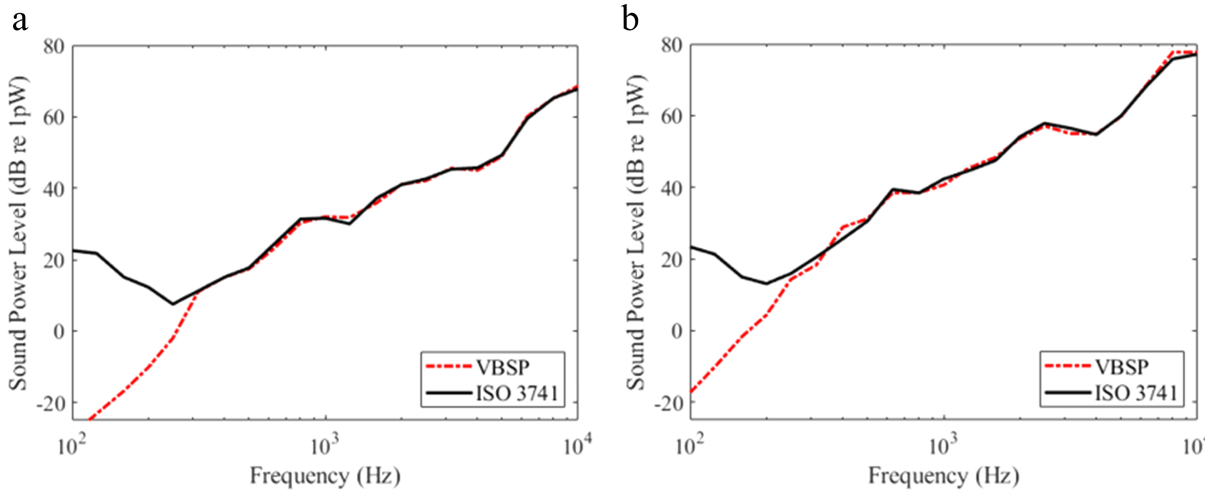


*Fig. 10—Results of the sound power measurements using the VBSP method compared to the ISO 3741 standard for (a) The TR curved plate and (b) The WR curved plate.*

pressure and is unable to distinguish between the noise produced from the curved plate and the background noise in the reverberation chamber at frequencies below the Schroeder frequency. Hence, the VBSP method is likely more accurate in measuring the sound power below the Schroeder frequency and when the noise source radiates below the noise floor of the reverberation chamber.

*Table 2—The absolute difference in sound power measurements for the MR, TR, and WR curved plates using the VBSP method and ISO 3741. Similarly, for the WR curved plate in two uncontrolled acoustic environments.*

| | | $\Delta L_w$ (dB re 1 pW) | | | | |
|---|---|---|---|---|---|---|
| Curved Plate | | MR | TR | WR | Hallway | Outside |
| OTO band frequency (Hz) | 100 | 42.3 | 51.5 | 40.7 | 38.3 | 35.4 |
| | 125 | 36.6 | 44.9 | 31.5 | 32.0 | 29.1 |
| | 160 | 25.1 | 31.9 | 16.7 | 19.1 | 18.9 |
| | 200 | 17.8 | 22.5 | 8.7 | 11.5 | 13.4 |
| | 250 | 8.5 | 9.5 | 1.6 | 6.0 | 6.8 |
| | 315 | 2.3 | 0.2 | 2.2 | 0.3 | 1.7 |
| | 400 | 0.1 | 0.0 | 3.3 | 2.4 | 0.2 |
| | 500 | 0.8 | 0.3 | 0.7 | 6.2 | 3.3 |
| | 630 | 0.6 | 1.2 | 1.0 | 2.2 | 1.8 |
| | 800 | 1.2 | 1.0 | 0.1 | 0.0 | 0.2 |
| | 1000 | 1.0 | 0.4 | 1.7 | 1.7 | 1.8 |
| | 1250 | 0.5 | 1.8 | 0.7 | 0.5 | 2.2 |
| | 1600 | 1.4 | 1.3 | 0.9 | 0.6 | 0.4 |
| | 2000 | 1.1 | 0.1 | 0.5 | 0.4 | 0.1 |
| | 2500 | 1.0 | 0.5 | 0.7 | 0.4 | 0.3 |
| | 3150 | 0.2 | 0.3 | 1.5 | 0.4 | 0.3 |
| | 4000 | 1.4 | 0.7 | 0.2 | 0.3 | 0.3 |
| | 5000 | 2.0 | 0.3 | 0.2 | 0.9 | 1.1 |
| | 6300 | 2.8 | 0.6 | 0.3 | 2.1 | 2.0 |
| | 8000 | 1.0 | 0.1 | 1.9 | 0.1 | 0.1 |
| | 10,000 | 1.2 | 0.8 | 0.6 | 0.5 | 0.6 |
| | **Overall** | **0.3** | **0.5** | **1.0** | **0.1** | **0.2** |

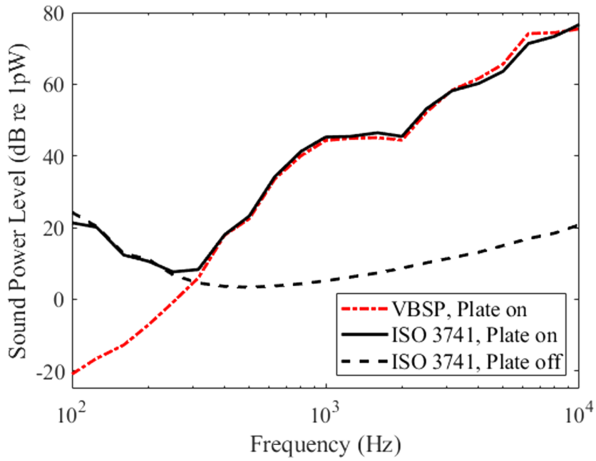


*Fig. 11—Results of the sound power measurements using the VBSP method compared to the ISO 3741 standard for the MR curved plate. Background noise results from the reverberation chamber are also included (ISO 3741, plate off).*

These results demonstrate that the VBSP method is likely able to measure sound power from specific devices in relatively noisy environments, reducing the need for specific acoustic environments such as anechoic and reverberation chambers.

Figure 11 displays the sound power measured from the MR curved plate using both the VBSP and ISO 3741 methods. Initially, the plate was excited, and sound power levels were measured using both methods. Subsequently, the excitation was deactivated to measure the background noise levels in the reverberation chamber using the ISO 3741 standard (indicated by black dashed lines).

The results show favorable agreement between the sound power methods across the 315 Hz to 10 kHz OTO bands. The maximum difference between the VBSP and ISO 3741 methods across the usable bandwidth (315 Hz to 10 kHz) was 2.8 dB at the 6.3 kHz OTO band. The mean difference was 0.2 dB with a standard deviation of 1.4 dB. For the full frequency spectrum (100 Hz to 10 kHz), the overall sound power level was 79.7 dB re $10^{-12}$ W using the VBSP method and 79.4 dB re $10^{-12}$ W using the ISO 3741 method, resulting in a total difference of 0.3 dB.

Below the 315 Hz OTO band, the two methods diverge, and there remains consistent agreement between the sound power measured from the MR curved plate using the ISO 3741 standard and the background noise in the chamber. This suggests that the ISO 3741 method predominantly measures the background noise of the reverberation chamber below 315 Hz, which masks the relatively low sound power output from the MR curved plate within this range[31].

In contrast, the VBSP method demonstrates significantly reduced sensitivity to the chamber's background noise. Therefore, it is likely that the VBSP method is the more accurate measurement down to 100 Hz.

## 4.2 Anechoic and Uncontrolled Acoustic Environments

Figure 12 compares the results from the ISO 3745 standard in the anechoic chamber with the VBSP results in the uncontrolled environments below the 400 Hz OTO band. They show good agreement between the methods down to the 160 Hz OTO band. The deviations in the sound power methods below 160 Hz come from the inability of the PZT excitation to produce sound pressure levels above the ISO 3745 standard's background noise criterion. It is likely that the methods would agree better with a stronger excitation below this OTO band. Further, this confirms that the VBSP method can indeed measure the sound power from baffled structures across the OTO bandwidth (160 Hz to 10 kHz).

The ISO 3741 method introduces significant error below the 315 Hz OTO band due to the noise floor, while the VBSP method demonstrates greater accuracy within this frequency range. The plate was remounted on the wall with a new PZT, so these results will not be the same as the VBSP results in the reverberation chamber. A new ISO 3741 measurement was taken and included in Fig. 12. Table 2 quantifies the OTO band sound power differences between the VBSP and ISO 3741 methods for the WR curved plate. These results confirm the robustness of the VBSP method in different environments and its capability of in situ testing.

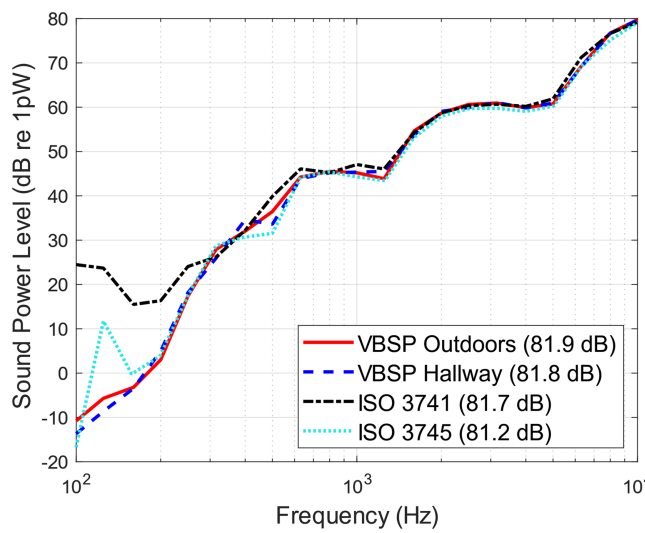


*Fig. 12—The VBSP results of the WR curved plate in two uncontrolled acoustic environments compared to the ISO 3741 and ISO 3745 standards.*

## 5 CONCLUSIONS

In this study, a VBSP method was developed and validated for measuring sound power from baffled simply curved plates. Previous research focused on **R** matrix expressions for baffled flat plates, fully closed cylindrical shells, and fully closed spherical shells, leaving a gap for open-curved plate geometries encountered in practical applications such as tractor cab windows, car door panels, and aircraft or marine vehicle panels.

Experimental validation was performed and involved comparing sound power obtained from the VBSP method using the new **R** matrix expression with the pressure-based ISO 3741 and ISO 3745 standards. Three curved plates with varying radii of curvature were fabricated and tested in several environments. Excellent agreement was observed between the VBSP method and ISO 3741 standard, in a reverberation chamber, within the usable bandwidth (400 Hz to 10 kHz OTO bands). The VBSP method exhibited lower sensitivity to background noise compared to the ISO 3741 standard. Mean sound power differences for the three plates, with respective standard deviations, were 0.2 dB (1.4 dB) for the MR curved plate, 0.1 dB (0.8 dB) for the TR curved plate, and 0.1 dB (2.1 dB) for the WR curved plate, when compared to the ISO 3741 standard.

Furthermore, the VBSP method demonstrated its capability to accurately measure sound power from the WR curved plate in non-controlled acoustic environments. Tests were conducted in a hallway with moderate foot traffic, loud HVAC system, and elevator noise, as well as outdoors with high vehicle noise, a rainstorm with thunderclaps, wind speeds up to 11 mph, and temperature variations of 14 °F (7.8 °C), showcasing the robustness of the VBSP method.

The sound power of the WR curved plate was then measured in an anechoic chamber according to the ISO 3745 standard. The results confirm the VBSP method's ability to capture the radiated energy below the threshold frequency of 385 Hz for the ISO 3741 standard in the reverberation chamber. Previous papers on the VBSP method have not confirmed this result due to restricting the testing in a reverberation chamber with a Schroeder frequency of 385 Hz. This result supports the claim that the VBSP method is likely measuring the sound power accurately below 400 Hz OTO band.

These results highlight the potential of the VBSP method for accurately measuring sound power from baffled simply curved plates, surpassing the limitations of traditional measurement standards in certain scenarios. The sound power from a baffled structure can be accurately measured using the VBSP method in different acoustic environments across the OTO bandwidth of interest (160 Hz to 10 kHz).

This work validates the robustness of the VBSP method in measuring sound power from baffled simply curved plates in real-world environments. The developed baffled simply curved plate **R** matrix expression enables the natural acoustic radiation modes for these structures to be computed. These results have significant implications for accurately characterizing the sound power of curved plates in various industrial applications. The results support the practical application of the VBSP method outside of controlled acoustic environments in situ, allowing for accurate sound power measurements even in the presence of significant background and time-varying noise produced by the plate environment, and provide confidence in the viability of the baffled simply curved plate **R** matrix for future use.

## 6 ACKNOWLEDGMENTS

The authors gratefully acknowledge the assistance of Jeremy Peterson and his machine shop for help with fabricating the curved plates and the wall for the anechoic chamber. Furthermore, the authors extend gratitude for the additional support from various BYU students and staff members with different aspects of the work presented here.

This work was partially supported by the National Science Foundation (grant number 1916696).

## 7 APPENDIX A

### 7.1 Introduction

A "special" function in mathematics is one that appears so often that it receives a name, and its properties are studied[23,25]. Many special functions cannot be expressed in terms of elementary functions and therefore can only be expressed in terms of integrals and differential equations[33]. This appendix was organized using Appendices B and V from Refs. 24 and 29, respectively, to define the special functions used within this article so that the article is more self-contained.

### 7.2 Bessel and Hankel Functions

The $v$th-order Bessel functions of the first and second kind are given by

$$J_v(x) = \sum_{m=0}^{\infty} (-1)^m \frac{x^{v+2m}}{m!(v+m)!} \tag{A.1}$$

and

$$Y_v(x) = \frac{J_v(x)\cos(\pi v) - J_{-v}(x)}{\sin(\pi v)}, \tag{A.2}$$

respectively.

The $v$th-order Hankel functions of the first and second kind are given by

$$H_v^{(1)}(x) = J_v(x) + jY_v(x) \tag{A.3}$$

and

$$H_v^{(2)}(x) = J_v(x) - jY_v(x), \tag{A.4}$$

respectively.

### 7.3 Fock-type Airy Function

In electromagnetics, the Fock-type Airy function[25] is given by

$$W_2(\tau) = \frac{1}{\sqrt{\pi}} \int_{C_2} e^{-\left(\frac{z^3}{3}\right)} e^{\tau z} dz \tag{A.5}$$

where $C_2$ is shown in Fig. A.1.

### 7.4 The Fock V Coupling Function

The hard Fock coupling function, denoted by $V(x)$, was developed to give an asymptotic description of the electric current over convex surfaces[33–35] and is given by

$$V(x) = \frac{\sqrt{x}\, e^{\frac{j\pi}{4}}}{2\sqrt{\pi}} \int_{\infty C_1}^{\infty} \frac{(W_2(\tau) e^{-jx\tau})}{W_2'(\tau)} d\tau. \tag{A.6}$$

$V(x) \in \mathbb{C}$ even though $x \in \mathbb{R}$. The contour of integration $C_1$ for Eqn. A.6 is shown in Fig. A.1.

Let $\tau_n = |\tau_n| e^{-\frac{j\pi}{3}}$ and $\tau_n' = |\tau_n'| e^{-\frac{j\pi}{3}}$. When $x > 0.6$, the first ten terms are usually sufficient to approximate $V(x)$ using the following expression[25]:

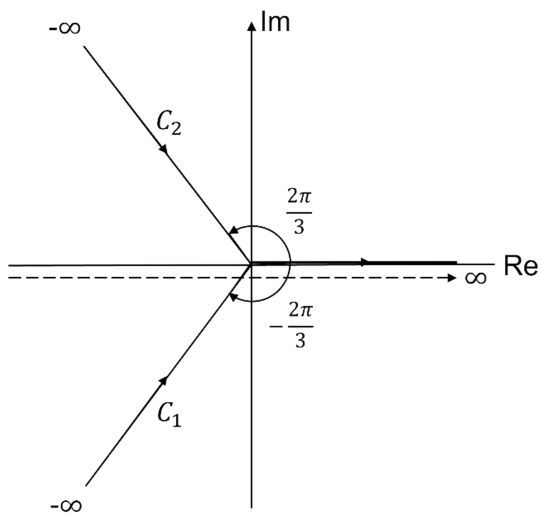


*Fig. A.1—Contours in the complex τ-plane for Fock V integration.*

*Table A.1—The First Ten Zeros of $W_2(\tau)$: $W_2(\tau_n') = 0$ and $W_2'(\tau_n) = 0$, where $\tau_n = |\tau_n| e^{-\frac{j\pi}{3}}$ and $\tau_n' = |\tau_n'| e^{-\frac{j\pi}{3}}$.*

| $n$ | $\lvert \tau_n \rvert$ | $\lvert \tau_n' \rvert$ |
|---|---|---|
| 1 | 2.33811 | 1.01879 |
| 2 | 4.08795 | 3.24819 |
| 3 | 5.52056 | 4.82010 |
| 4 | 6.78661 | 6.16331 |
| 5 | 7.94413 | 7.37218 |
| 6 | 9.02265 | 8.48849 |
| 7 | 10.0402 | 9.53545 |
| 8 | 11.0085 | 10.5277 |
| 9 | 11.9300 | 11.4751 |
| 10 | 12.8288 | 12.3848 |

$$V(x) \approx \sqrt{\pi x}\, e^{-\frac{j\pi}{4}} \sum_{n=1}^{10} \frac{e^{-jx\tau_n'}}{\tau_n'} \tag{A.7}$$

where the $\tau_n'$ values are given in Table A.1. When $x < 0.6$, then the first four terms are usually sufficient to approximate $v(x)$ using the following expression[25]

$$V(x) \approx 1 - \frac{\sqrt{\pi}}{4} e^{\frac{j\pi}{4}} x^{\frac{3}{2}} + \frac{7j}{60} x^3 + \frac{7\sqrt{\pi}}{512} x^{\frac{9}{2}}. \tag{A.8}$$

## 8 REFERENCES


1. G.V. Borgiotti, "The power radiated by a vibrating body in an acoustic fluid and its determination from boundary measurements", *J. Acoust. Soc. Am.*, **88**(4), 1884–1893, (1990).
2. S.J. Elliot and M.E. Johnson, "Radiation modes and the active control of sound power", *J. Acoust. Soc. Am.*, **94**(4), 2194–2204, (1993).
3. A. Sarkissian, "Acoustic radiation from finite structures", *J. Acoust. Soc. Am.*, **90**, 574–578, (1991).
4. K. A. Cunefare and M. N. Currey, "On the exterior acoustic radiation modes of structures," *J. Acoust. Soc. Am.*, **96**(4), 2302–2312, (1994).
5. F. Fahy and P. Gardonio, *Sound and Structural Vibration: Radiation, Transmission and Response*, 2nd edn, Academic Press, Oxford, UK, (2007): 165–175.
6. J.P. Arenas and M.J. Crocker, "Sound radiation efficiency of a baffled rectangular plate excited by harmonic point forces using its surface resistance matrix", *Int. J. Acoust. Vib.*, **7**(4), 217–229, (2002).
7. A. Loghmani, M. Danesh, M.K. Kwak, and M. Keshmiri, "Active control of radiated sound power of a smart cylindrical shell based on radiation modes", *Appl. Acoust.*, **114**, 218–229, (2016).
8. J. Liu, Y. Liu, and J.S. Bolton, "Acoustic source reconstruction and visualization based on acoustic radiation modes", *J. Sound Vib.*, **437**, 358–372, (2018).
9. C.B. Goates, S.D. Sommerfeldt, and J.D. Blotter, "Frequency trends of acoustic radiation modes for cylindrical structures", *Proc. Mtgs. Acoust.*, **35**(1), 065003, (2018).
10. C.B. Goates, C.B. Jones, S.D. Sommerfeldt, and J.D. Blotter, "Sound power of vibrating cylinders using the radiation resistance

matrix and a laser vibrometer", *J. Acoust. Soc. Am.*, **148**(6), 3553–3561, (2020).
11. C.B. Jones, C.B. Goates, J.D. Blotter, and S.D. Sommerfeldt, "Experimental validation of determining sound power using acoustic radiation modes and a laser vibrometer", *Appl. Acoust.*, **164**, 107254, (2020).
12. I.C. Bacon, S.D. Sommerfeldt, and J.D. Blotter, "Developing an indirect vibration-based sound power method to determine the sound power radiated from acoustic sources", *Proc. Mtgs. Acoust.*, **50**(1), 065003, (2022).
13. M.R. Bai and M. Tsao, "Estimation of sound power of baffled planar sources using radiation matrices", *J. Acoust. Soc. Am.*, **112**, 876–883, (2002).
14. W.R. Johnson, P. Aslani, S.D. Sommerfeldt, J.D. Blotter, and K.L. Gee, "Acoustic radiation mode shapes for control of plates and shells", *Proc. Mtgs. Acoust.*, **19**(1), 065036, (2013).
15. G.V. Borgiotti and K.E. Jones, "Frequency independence property of radiation spatial filters", *J. Acoust. Soc. Am.*, **96**(6), 3516–3524, (1994).
16. Y. Sun, T. Yang, and Y. Chen, "Sound radiation modes of cylindrical surfaces and their application to vibro-acoustics analysis of cylindrical shells", *J. Sound Vib.*, **424**, 64–77, (2018).
17. D.M. Photiadis, "The relationship of singular value decomposition to wave-vector filtering in sound radiation problems", *J. Acoust. Soc. Am.*, **88**(2), 1152–1159, (1990).
18. H. Wu, W. Jiang, and Y. Zhang, "A method to compute the radiated sound power based on mapped acoustic radiation modes", *J. Acoust. Soc. Am.*, **135**, 679, (2014).
19. K.A. Cunefare, M.N. Currey, M.E. Johnson, and S.J. Elliott, "The radiation efficiency grouping of free-space acoustic radiation modes", *J. Acoust. Soc. Am.*, **109**, 203–215, (2001).
20. T.P. Bates, I.C. Bacon, J.D. Blotter, and S.D. Sommerfeldt, "Vibration-based sound power measurements of arbitrarily curved panels", *J. Acoust. Soc. Am.*, **151**, 1171–1179, (2022).
21. ISO 3741:2010, *Acoustics — Determination of sound power levels and sound energy levels of noise sources using sound pressure — precision methods for reverberation test rooms,* International Organization for Standardization, (Geneva, Switzerland, 2010).
22. ISO 3745:2012, *Acoustics — Determination of sound power levels and sound energy levels of noise sources using sound pressure — precision methods for anechoic rooms and hemi-anechoic rooms,* International Organization for Standardization, (Geneva, Switzerland, 2012).
23. C.B. Goates, Analytical Expressions for Acoustic Radiation Modes of Simple Curved Structures, Master's Thesis, Brigham Young University, Provo, UT, 2019.
24. D.A. McNamara, J.A.G. Malherbe, and C.W. Pistorius, Introduction to the uniform geometrical theory of diffraction, Artech House, Boston, MA, 422–433, (1990).
25. P.H. Pathak and N.N. Wang, "Ray analysis of mutual coupling between antennas on a convex surface", *IEEE Trans. Ant. Prop.*, **29**(6), 911–922, (1981).
26. T.A. Pitts, R.H. Selfridge, and D.M. Bhabries, "Solution of the Euler field equations for plane-wave scattering by an end-capped cylinder via the uniform geometrical theory of diffraction", *J. Acoust. Soc. Am.*, **94**(6), 3437–3447, (1993).
27. B.R. Levy and B.J. Keller, "Diffraction by a smooth object", *Comm. Pur. Appl. Math.*, **12**(1), 159–209, (1959).
28. A.S. Fokas and E.A. Spence, "Synthesis, as opposed to separation, of variables", *SIAM Review*, **54**(2), 291–324, (2012).
29. G.N. Watson, "The diffraction of electric waves by the earth", *Proc. R. Soc. Lond. A*, **95**, 83–99, (1918).
30. P.H. Pathak and N.N. Wang, "An analysis of the mutual coupling between antennas on a smooth convex surface," Tech. Report 784583-7, Ohio State University Columbus Electroscience Lab (1978).
31. T.P. Bates, I.C. Bacon, C.B. Goates, S.D. Sommerfeldt, and J.D. Blotter, "Experimental sound power from curved plates using the radiation resistance matrix and a scanning vibrometer", *InterNoise21*, 2755–2766, (2021).
32. T.W. Leishman, S. Rollins, and H.M. Smith, "An experimental evaluation of regular polyhedron loudspeakers as omnidirectional sources of sound", *J. Acoust. Soc. Am.*, **120**(3), 1411–1422, (2006).
33. S. Hassani, *Mathematical Physics: A Modern Introduction to Its Foundations*, 2nd edn, Cham: Springer, (2013), p. 437.
34. T. Bird, "Accurate asymptotic solution for the surface field due to apertures in a conducting cylinder", *IEEE Trans. Ant. Prop.*, **33**(10), 1108–1117, (1985).
35. S. Bird, "Appendix D: properties of surface fock functions", in *Mutual Coupling Between Antennas*, 429–432, (2021).